Avoided crossings of diamagnetic hydrogen as functions of magnetic field strength and angular momentum

J. R. Walkup, M. Dunn, and D. K. Watson
Department of Physics and Astronomy, University of Oklahoma, Norman, Oklahoma 73019

T. C. Germann
Theoretical Division (T-11), Los Alamos National Laboratory, Los Alamos, New Mexico 87545
(Received 24 February 1998)

The energy levels of diamagnetic hydrogen as a function of two independent parameters, magnetic field strength B, and angular momentum m, are examined. Avoided crossings appear between these energy levels as either parameter is varied while the other is held fixed. These avoided crossings are directly related to degeneracies (Fermi resonances) occurring at zeroth order in perturbation theory. The mathematical basis of these degeneracies are the square-root branch points that connect the energy levels. It is found that the locations of avoided crossings in either constant-B or constant-m spectra can be predicted by visually scanning the locations of these branch points in the complex-δ plane, where $\delta = 1/(2+2|m|)$ is the perturbation parameter used in this research. [S1050-2947(98)07111-X]

PACS number(s): 32.80.Bx, 32.60.+i, 31.15.Md, 32.30.−r

I. INTRODUCTION

Those wanting a stark contrast between the words *simple* and *easy* need look no further than the diamagnetic hydrogen problem. While simple in description, such a problem has defied analytic solution [1–5]. The system, a hydrogen atom placed in a constant magnetic field B oriented along a fixed axis, has numerous applications and analogs in such diverse fields as astrophysics [1,6] and solid-state physics [7]. The interest in astrophysical applications was prompted by the discovery of strong magnetic fields in certain white dwarfs and neutron stars. In solid-state physics excitons behave in many respects like hydrogenic atoms. Due to the reduced effective mass of the electron in such a system, a laboratory-strength magnetic field in practice can mimic the effects of a much stronger magnetic field on diamagnetic hydrogen.

Because it is a nonlinear system with two nonintegrable degrees of freedom, diamagnetic hydrogen is also an important experimentally accessible test case for studying quantum chaos [3,5,8]. The Rydberg states of diamagnetic hydrogen are particularly interesting [4,5,9,10]. Many of these states play an especially important role in studying quantum chaos because their highly excited nature renders them quite suitable to study with laboratory-strength magnetic fields [11]. *Circular* Rydberg states, those with large $|m|$ values such that $n = |m| + 1$, are also important because they are experimentally accessible and relatively long lived [12].

The coupling between the two degrees of freedom, caused by the Coulombic and diamagnetic terms, produces a nonseparable Hamiltonian, thwarting all attempts to find analytic solutions to the diamagnetic hydrogen problem. This coupling creates a markedly different energy ordering in two important extremes of B: For $B = 0$ the energy spectrum is hydrogenic, while at sufficiently large B the energy levels divide into a series of Landau channels (see [13] for example). These channels are supported by the same radial wave functions describing motion perpendicular to a magnetic field, as are found for a free electron in a magnetic field. Between these two limits of B the interplay between the Coulomb and diamagnetic contributions creates a complicated, often highly irregular, energy spectrum. Each energy level is perturbed from above and below by adjacent levels as the system evolves from the hydrogenic to Landau limits and so the response of the system as B is increased is necessarily quite complex. Even for very low B the diamagnetic term generates ℓ mixing in each hydrogenic n manifold.

The most distinctive feature of the response of the energy spectrum to adiabatic changes in the B field is an intricate array of avoided crossings [14], which provide the mechanism for state reordering with energy E as B is changed. By this we mean that, at least in the nonchaotic region [15], the characters of the states exchange diabatically as the system is taken through the avoided crossings by varying the external magnetic field. However, the appearance of avoided crossings is not restricted merely to variations in B. In the particular system we have chosen to study, the angular-momentum quantum number m is a conserved quantity because of the separability of the azimuthal degree of freedom. We show that avoided crossings also appear in the energy spectrum as m of the system is incremented in value. (Actually, we treat m in this paper as a continuously varying real parameter, interpolated between integer values.) As when B is varied for fixed m, the characters of the states diabatically exchange across the avoided crossings when m is varied [16].

Avoided crossings are not always easy to distinguish. Some are so sharp that energy levels superficially appear to actually cross. (Energy levels with the same parity and m cannot cross because of the Wigner–von Neumann noncrossing rule [17].) On the other hand, some avoided crossings are so broad that they are not easily discernible. These are

termed *hidden* avoided crossings [18,19]. Regardless of whether or not they are hidden, the characters of the wave functions still exchange diabatically across the avoided crossings. Because of this very important physical effect, it is important to have a rationale for the existence of avoided crossings to predict roughly where they occur, hidden or not. In this paper we offer such a rationale, which relies on understanding the mathematical structure resulting from degeneracies between energy levels. Furthermore, we can use the *same* mechanism that explains the appearance of avoided crossings in the E-versus-B spectrum to understand those appearing in the E-versus-$|m|$ spectrum as well. *Therefore, this mechanism directly relates the response of the energy to independent changes in B and* $|m|$.

To analyze the avoided crossings appearing in the energy spectrum of diamagnetic hydrogen we use dimensional perturbation theory [20], which in the system we are considering is equivalent to angular-momentum ($|m|$) perturbation theory [21]. However, unlike angular-momentum perturbation theory, this method is applicable to a wider range of more complex problems. To date, dimensional perturbation theory has been applied to such diverse fields as statistical mechanics, nuclear and particle physics, quantum optics, and atomic and molecular physics [20,22–24]. In atomic and molecular physics alone dimensional perturbation theory has been applied to atomic Zeeman and Stark effects [20,24,25], van der Waals coefficients [26], the hydrogen atom in parallel electric and magnetic fields [27,28], two-electron and many-electron atoms, ions, and molecules [20,29], quasistationary states [24,27,30], potential scattering problems [25,31], and density-functional theory [32], to name just a few. Furthermore, projects are currently under way using this theory to compute the rotational spectra of molecules [33] and virial coefficients and phase transitions in the electronic structure of atoms and molecules [34].

Dimensional perturbation theory not only is a potent method for calculating energies and other properties of many quantum-mechanical systems [20,35] but also provides a natural way of examining avoided crossings in diamagnetic hydrogen energy levels. With this method, the magnetic field and Coulomb potential are both incorporated into the Hamiltonian at zeroth order to such an extent that we can directly associate avoided crossings appearing in the E-versus-B spectrum with degeneracies arising at zeroth order. Therefore, this method establishes an orderly means of examining the complicated energy spectrum of diamagnetic hydrogen. Also, all angular-momentum dependence of the problem is contained within the perturbation parameter, which we denote in this paper as δ. Changing m merely amounts to resumming the energy series at a different value of δ, which is *considerably* easier than a new calculation required by other methods. This greatly simplifies examining energy levels as a function of angular momentum.

In this paper we examine the degeneracies of diamagnetic hydrogen for two characteristic energy-level interactions and from this information we explain the existence and locations of some low-lying avoided crossings appearing in its energy spectrum. In Sec. II we consider a simple example in which a system parameter is varied adiabatically. We then explain how the resulting avoided crossing in the energy spectrum is related to square-root branch point degeneracies appearing in the complex parameter-plane. In Sec. III we formulate the dimensional perturbation theory used in this research. Using the resulting energy series, in Sec. IV we plot energy levels as functions of magnetic-field strengths at two different orders in perturbation theory: harmonic (zeroth) order and higher (28th) order. We show that we can relate the avoided crossings appearing in the energy spectrum to energy degeneracies appearing at harmonic order, as expected.

In Sec. V we instead fix B and plot energy levels as the *angular momentum* $|m|$ is changed. We show that the avoided crossings appearing in this situation are directly related to those appearing in the E-versus-B spectrum. As demonstrated in Ref. [36], this relationship is illuminated by examining the anatomy of the branch point degeneracies connecting the two energy levels in question. We use this anatomy in Sec. VI to predict the appearance of avoided crossings in both types of spectra.

We expect the analysis in Sec. VI to apply to all avoided crossings appearing throughout the energy spectra (both E-versus-B and E-versus-m spectra) of diamagnetic hydrogen. However, there is one small subset of avoided crossings that demands expanded treatment and we consider this subset of avoided crossings in Sec. VII.

This paper focuses solely on examining the odd-parity states of diamagnetic hydrogen. As we explain in Sec. VIII, all results apply to the even-parity states equally well.

II. ENERGY DEGENERACIES AND AVOIDED CROSSINGS

To illustrate the relationship between energy degeneracies and avoided crossings, we use an example much like the one discussed by Bender and Orszag [37]. Consider the time-independent Schrödinger equation of a simple two-level system,

$$\mathcal{H}\Psi_{\pm}=E^{\pm}\Psi_{\pm}, \tag{1}$$

where

$$\mathcal{H}=\begin{pmatrix} b & c \\ c & d \end{pmatrix}. \tag{2}$$

Here we consider b, which is analogous to B or m in this paper, as a variable parameter. Equation (1) models a general quantum-mechanical problem in those regions where only two states interact strongly enough to warrant consideration. If $d=-b$, then Eq. (1) models a well-known Landau-Zener problem [38], where b is associated with a linearly varying, time-dependent magnetic field and c measures the splitting between energy levels caused by a constant magnetic field oriented perpendicular to the first. The energy eigenvalues as functions of b are plotted in Fig. 1, which shows an avoided crossing centered about $b=d$. As $b\rightarrow\pm\infty$, the energies E^{+} and E^{-} and the eigenstates Ψ_{+} and Ψ_{-} approach the $c=0$ solutions

$$\phi_1=\begin{pmatrix} 1 \\ 0 \end{pmatrix} \tag{3}$$

with energy $E_1=b$ and

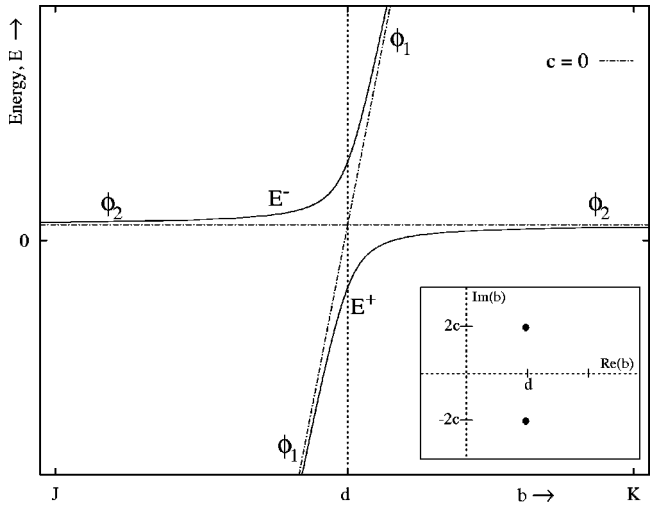

FIG. 1. Energy levels E^+ (lower level) and E^- (upper level) arising from Eq. (1), with b treated as a variable parameter. Note that the characters of the states, defined as either ϕ_1 or ϕ_2, exchange diabatically as the system progresses through the avoided crossing. In other words, if we (infinitely slowly) increase b from J to K, the state corresponding to the E^+ level would transform from ϕ_1 to ϕ_2 in the avoided crossing region. For $c=0$ the system becomes separable and so at this limit the energy levels (shown by dot-dashed lines) cross at $b=d$. The inset shows the square-root branch points lying in the complex-b plane that connect the two energy levels.

$$\phi_2=\begin{pmatrix}0\\1\end{pmatrix} \tag{4}$$

with energy $E_2=d$. Thus, when b is sufficiently far from the avoided crossing center the energies and eigenstates are approximated by the $c=0$ energies and eigenstates. We use ϕ_1 and ϕ_2 to label the character of the finite-b eigenstates away from the avoided crossings. Since the energy ordering of the $c=0$ eigenstates ϕ_1 and ϕ_2 is different from one extreme value of b to the other, the states must exchange character diabatically across the avoided crossing. If the character of the state defined by ϕ_2 is associated with the *upper* energy level E^- when $b \ll d$, then ϕ_1 will associate with the *lower* level E^+. However, this ordering of states reverses for $b \gg d$ and so the characters of both energy levels exchange across the avoided crossing.

In this example the avoided crossing is clearly visible in the energy spectrum, but as we stated previously such is not always the case. Yet the existence of hidden avoided crossings remains physically important since the character of each interacting energy level exchanges when the system passes through the avoided crossing. Therefore, it is important to find a distinguishing characteristic of the system that signifies the locations of avoided crossings, whether or not they are hidden.

From Eqs. (1) and (2) we can write the secular equation in the form

$$(E-E^+)(E-E^-)=E^2-(E^++E^-)E+E^+E^-=0, \tag{5}$$

where

$$E^++E^-=b+d, \quad E^+E^-=bd-c^2. \tag{6}$$

The avoided crossing occurs when the parameter b passes closest to where the two eigenenergies are degenerate. According to Eqs. (6), in order for $E^+=E^-$ the parameter b must satisfy $b^2-2db+4c^2+d^2=0$, that is,

$$b^{\pm}=d\pm 2ic. \tag{7}$$

Note that the degeneracies occur at complex values of b; physical (real-valued) energies cannot cross as b is held on the real line and swept past the degeneracy points. (The Schwarz reflection principle [39] ensures that degeneracies occur at *complex-conjugate* values of b.) Rather, as shown in Fig. 1, we see an avoided crossing centered about $b=d$ because the energies come closest to degeneracy when b is closest to d.

The analytic solutions for the eigenenergies are

$$E_{\pm}=\frac{1}{2}[b+d\pm\sqrt{b^2-2db+4c^2+d^2}]; \tag{8}$$

thus we find square-root branch point singularities at the points where the energies are degenerate [40]. In other words, *the two square-root branch points provide a signature for the appearance of avoided crossings*. (See the inset in Fig. 1.)

A square root appeared in Eq. (8) because we considered an interaction between only two levels. When three levels interact, one might think that the degeneracies would be marked by both cube-root and square-root branch points. However, as explained by Bender and Orszag, higher-order, three-state degeneracies at which cube-root singularities can occur are extremely unlikely [37]. This reasoning applies to degeneracies and higher-order singularities involving more than three states as well. Therefore, as a general rule avoided crossings will be marked by the nearby presence of *square-root* branch points no matter how many states effectively interact [41].

Naturally, we cannot properly describe diamagnetic hydrogen with a simple 2×2 matrix equation, but rather we require an infinite-dimensional matrix equation, limited to finite dimensions for practicality. Dimensional perturbation theory, when formulated in the matrix method [23] (the method used for large-order calculations in this paper), automatically furnishes matrix equations of finite dimension at finite order. However, as we increase the rank of the matrix equation it is natural to question what correspondingly happens to the square-root branch point structure of the system. There are at least four possibilities [37]: (i) The square-root branch points stabilize and (a) remain well separated from each other or (b) form a sequence that becomes denser and denser towards some limiting point; (ii) the square-root branch points coalesce to form more complex singularities in the limit of infinite-dimensional matrices; (iii) the square-root branch points move to infinity; and (iv) a square root branch point present when the matrix equation is of a certain dimensionality is not present at other dimensionalities. We are only interested in avoided crossings that stabilize as the dimension of the matrix equation is increased and thus we rule out square-root branch points that behave as in items (iii) and (iv). As we shall see, for the energy-level interac-

tions considered in this paper the nearby square-root branch point degeneracies behave as in item (ia).

Finally, we note that for simple two-level systems Eq. (7) requires that real-valued branch points must exist at the same location on the real axis [42]. However, for higher ranking matrix equations this requirement no longer applies: Real-valued branch points can exist at two different points on the real line.

III. FORMULATION OF THE DIMENSIONAL PERTURBATION THEORY

The basic steps involved in all dimensional scaling methods, including dimensional perturbation theory, is to generalize the system to D spatial dimensions and subsequently scale the physical variables to remove the leading D dependence [20]. In the case of dimensional perturbation theory the scaled Schrödinger equation is expanded in a perturbation series about a value of D that allows an analytic solution. With diamagnetic hydrogen (as for many systems) the infinite-dimensional limit serves this purpose well. To find the energy corresponding to the three-dimensional system the perturbation series is simply summed at the value $D=3$ because all D dependence is incorporated into the perturbation parameter.

The generalization of the Schrödinger equation describing a hydrogenic atom in a constant magnetic field B to D dimensions is [20]

$$\left\{-\frac{1}{2}\left(\frac{\partial^2}{\partial\rho^2}+\frac{\partial^2}{\partial z^2}\right)+\frac{\kappa^2-4\kappa+3}{8\rho^2}+\frac{B^2\rho^2}{8}-\frac{Z}{r}\right\}\Phi(\rho,z) =E(\rho,z)\Phi(\rho,z), \tag{9}$$

$$\kappa\equiv D+2|m|-1, \tag{10}$$

where the field strength B is measured in units of 2.35×10^9 G and the time-independent wave function $\Psi(\rho,z)$ is dimensionally scaled as $\Phi(\rho,z)=\rho^{(\kappa-1)/2}\Psi(\rho,z)$. (We omit the normal Zeeman term since it does not affect the dynamics of the problem.) Here ρ and z are the D-dimensional generalization of the usual cylindrical coordinates and the remaining $D-2$ angular coordinates have been factored out to yield the ρ^{-2} centrifugal potential term. Note that D and $|m|$ only enter the Schrödinger equation through κ.

To obtain a useful infinite-dimensional limit some of the physical quantities must be dimensionally scaled:

$$\tilde{\rho}=\frac{\rho}{\kappa^2},\quad \tilde{z}=\frac{z}{\kappa^2},\quad \tilde{E}=\kappa^2E,\quad \tilde{B}=\kappa^3B. \tag{11}$$

Note that the conversion between B and $\tilde{B}$ in three dimensions is

$$B\ \text{(T)}\simeq\frac{2.94\times10^4}{(1+|m|)^3}\tilde{B}. \tag{12}$$

For example, 100 scaled units roughly equates to 75 T in three dimensions when $|m|=33$.

With these scaled quantities the Schrödinger equation has the form $\mathcal{H}\Phi=\tilde{E}\Phi$, where

$$\mathcal{H}=-\frac{1}{2}\delta^2\left(\frac{\partial^2}{\partial\tilde{\rho}^2}+\frac{\partial^2}{\partial\tilde{z}^2}\right)+\tilde{V}_{eff}, \tag{13}$$

$$\tilde{V}_{eff}=\frac{1-4\delta+3\delta^2}{8\tilde{\rho}^2}+\frac{\tilde{B}^2\tilde{\rho}^2}{8}-\frac{Z}{\sqrt{\tilde{\rho}^2+\tilde{z}^2}}. \tag{14}$$

Note that we introduced the perturbation parameter

$$\delta\equiv\frac{1}{\kappa}=\frac{1}{D+2|m|-1} \tag{15}$$

into the Hamiltonian. It is important to note that, as with κ, all D and m dependence is accounted for in δ.

As $\kappa\to\infty$ ($\delta\to0$) all derivative terms in the Hamiltonian vanish, producing an ''electrostatic'' problem; the electron settles to the minimum of the $\lim_{\delta\to0}\tilde{V}_{eff}(\tilde{\rho},\tilde{z})$ located at $(\tilde{\rho},\tilde{z})=(\rho_m,z_m=0)$. We denote the energy in the large-κ limit, i.e., $\lim_{\delta\to0}\tilde{V}_{eff}(\rho_m,z_m)$, by $\tilde{E}_\infty$. Therefore, in the large-κ limit (large-D and/or -$|m|$ limit) the electron of energy $\tilde{E}_\infty$ is constrained to a hypercircle of radius $\tilde{\rho}=\rho_m$ perpendicular to the $\hat{z}$ axis.

Using dimensionally scaled displacements x_1 and x_2, the origin is shifted to this minimum by means of the relations

$$\tilde{\rho}=\rho_m+\delta^{1/2}x_1,\quad \tilde{z}=\delta^{1/2}x_2. \tag{16}$$

The Schrödinger equation is then expanded in powers of $\delta^{1/2}$,

$$\tilde{E}=\tilde{E}_\infty+\sum_{i=0}^{\infty}\tilde{E}_{2i}\delta^{i+1}, \tag{17}$$

$$\mathcal{H}(\tilde{\rho},\tilde{z})=\tilde{E}_\infty+\sum_{i=0}^{\infty}\mathcal{H}_i(x_1,x_2)\,\delta^{(i/2)+1}, \tag{18}$$

$$\Phi(\tilde{\rho},\tilde{z})=\Phi_0(x_1,x_2)+\sum_{i=1}^{\infty}\Phi_i(x_1,x_2)\,\delta^{i/2}. \tag{19}$$

By equating powers of $\delta^{1/2}$ we obtain an infinite set of coupled differential equations

$$\sum_{j=0}^{p}(\mathcal{H}_j-\tilde{E}_j)\Phi_{p-j}=0,\quad \tilde{E}_{2i+1}=0,\quad p=0,1,2,\ldots. \tag{20}$$

The general form of $\mathcal{H}_j$ is given in Refs. [23,43]. Equations (17)–(20) can then be solved for the expansion coefficients $\tilde{E}_i$ and $\Phi_i(x_1,x_2)$. Of immediate importance is the solution for zeroth-order (harmonic) wave functions. When $p=0$ in Eq. (20) we obtain $(\mathcal{H}_0-\tilde{E}_0)\Phi_0=0$, where

$$\mathcal{H}_0=-\frac{1}{2}\left(\frac{\partial^2}{\partial x_1^2}+\frac{\partial^2}{\partial x_2^2}\right)+\frac{1}{2}\omega_1^2x_1^2+\frac{1}{2}\omega_2^2x_2^2-\frac{1}{2\rho_m^2} \tag{21}$$

has been put into the same form as a two-dimensional simple harmonic oscillator (SHO) by defining the so-called Langmuir oscillation frequencies

TABLE I. Fermi resonances and corresponding interacting states appearing in the harmonic-order energy spectrum in Fig. 2, with the lowest-energy interactions appearing highest in the table. The (scaled) magnetic-field strength at which each resonance appears is given in parentheses, rounded to the nearest whole number. Each entry corresponds to an individual interaction, many of which involve more than two states. Any even-parity states that are degenerate to those listed were omitted. Also, some of the higher-lying Fermi resonances in Fig. 2 were omitted for brevity.

8:7 (5)	6:5 (6)	4:3 (9)	3:2 (13)	8:5 (16)	2:1 (32)	8:3 (79)	3:1 (118)	4:1 (321)
$\|09\rangle,\|71\rangle$	$\|07\rangle,\|51\rangle$	$\|05\rangle,\|31\rangle$	$\|07\rangle,\|41\rangle$	$\|09\rangle,\|51\rangle$	$\|03\rangle,\|11\rangle$	$\|09\rangle,\|31\rangle$	$\|07\rangle,\|21\rangle$	$\|05\rangle,\|11\rangle$
$\|19\rangle,\|81\rangle$	$\|17\rangle,\|61\rangle$	$\|15\rangle,\|41\rangle$	$\|17\rangle,\|51\rangle$	$\|19\rangle,\|61\rangle$	$\|05\rangle,\|21\rangle$	$\|19\rangle,\|41\rangle$	$\|09\rangle,\|23\rangle$	$\|07\rangle,\|13\rangle$
	$\|09\rangle,\|53\rangle$	$\|07\rangle,\|33\rangle$	$\|09\rangle,\|43\rangle$		$\|07\rangle,\|15\rangle,\|23\rangle,\|31\rangle$		$\|17\rangle,\|31\rangle$	$\|09\rangle,\|15\rangle,\|21\rangle$
	$\|27\rangle,\|71\rangle$	$\|25\rangle,\|51\rangle$	$\|27\rangle,\|61\rangle$		$\|09\rangle,\|17\rangle,\|25\rangle,\|33\rangle,\|41\rangle$		$\|19\rangle,\|33\rangle$	$\|17\rangle,\|23\rangle$
	$\|19\rangle,\|63\rangle$	$\|17\rangle,\|43\rangle$	$\|19\rangle,\|53\rangle$		$\|19\rangle,\|27\rangle,\|35\rangle,\|43\rangle,\|51\rangle$		$\|27\rangle,\|41\rangle$	$\|19\rangle,\|25\rangle,\|31\rangle$

$$\omega_1^2=\frac{3}{4\rho_m^4}-\frac{2Z}{\rho_m^3}+\frac{\tilde{B}^2}{4},\quad \omega_2^2=\frac{Z}{\rho_m^3}. \tag{22}$$

The harmonic zeroth-order wave function Φ_0 (which describes quantum fluctuations about the large-κ limit) not only automatically adapts as B changes but adapts in a way that is sensitive to the interplay between the Coulombic and diamagnetic potentials. Therefore, dimensional perturbation theory is applicable to the entire range of magnetic-field strengths, not just to the high- or low-field regions.

Since Eq. (20) for $p=0$ is a two-dimensional SHO equation for $\Phi_0(x_1,x_2)$, to this harmonic order the energy is simply

$$\tilde{E}\approx\tilde{E}_\infty+\delta\tilde{E}_0=\tilde{E}_\infty+\delta\left(\left(\nu_1+\frac{1}{2}\right)\omega_1+\left(\nu_2+\frac{1}{2}\right)\omega_2-\frac{1}{2\rho_m^2}\right). \tag{23}$$

We assign the ket

$$|\nu_1\nu_2\rangle\equiv\Phi_0(x_1,x_2)=h_{\nu_1}(\sqrt{\omega_1}x_1)h_{\nu_2}(\sqrt{\omega_2}x_2) \tag{24}$$

to represent the ''unperturbed'' harmonic basis, where the ν_i are the quantum numbers of the SHO eigenfunctions $h_{\nu_i}(x)$. The quantum numbers ν_1 and ν_2 are the numbers of nodal lines in the $\hat{z}$ direction and nodes in the $\hat{\rho}$ direction, respectively. The basic topology of nodal lines is preserved at finite κ with the provision that states are traced diabatically across avoided crossings. Thus we use the quantum numbers ν_1 and ν_2 to label the *character* of the state corresponding to a particular energy level in the same way that the character of the states of the model problem in Sec. II for a particular value of b was labeled by ϕ_1 or ϕ_2.

The system parity π_z, which refers to reflection in the z coordinate, is determined by the value of ν_2: *Even-parity* states correspond to *even* values of ν_2 and likewise for odd-parity states. Although we largely limit the following discussion to examining odd-parity states, the response of the system described by Eq. (9) to adiabatic changes in $\tilde{B}$, most importantly the energy spectra and branch point trajectories as functions of $\tilde{B}$, are qualitatively the same no matter which parity sector we choose to consider.

In the next section we discover a one-to-one correspondence between the avoided crossings in the E-versus-B and the E-versus-$|m|$ spectra. To illustrate this relationship, we only need to look at a couple of avoided crossings in each of the E-versus-B and E-versus-$|m|$ spectra in detail. Because the perturbation parameter δ in Eq. (15) is especially small when $|m|$ is large, dimensional perturbation theory is particularly easy to apply to circular Rydberg states [43]. For that reason, we now apply dimensional perturbation theory to circular and near-circular states of diamagnetic hydrogen [44] and see how the system energy $E(\tilde{B},|m|)$ responds as both the magnetic-field strength $\tilde{B}$ (Sec. IV) and angular momentum $|m|$ (Sec. V) independently change.

IV. ENERGY AS A FUNCTION OF MAGNETIC-FIELD STRENGTH

The harmonic limit not only is mathematically useful but incorporates many features of the three-dimensional system. In fact, the harmonic Hamiltonian incorporates the effects of $\tilde{B}$ to such an extent that the ordering of states, with respect to energy, correlates exactly with that in three dimensions in both the small-$\tilde{B}$ and $\tilde{B}\to\infty$ limits. This is a key result because if the harmonic energy spectrum has the same basic structure as the exact spectrum, then we maintain the same energy-level ordering as higher-order corrections are incorporated, making the spectrum easier to examine. This is a major advantage of dimensional perturbation theory over many traditional methods.

The harmonic (zeroth-order) Hamiltonian $\mathcal{H}_0$ also is completely separable in $\hat{\rho}$ and $\hat{z}$, that is, the $\hat{\rho}$ and $\hat{z}$ degrees of freedom are uncoupled. This has important consequences for the harmonic energy spectrum that results from Eq. (23). The following are shown in Fig. 2 (for odd-parity states).

(i) The harmonic energy levels do not interact and actually cross.

(ii) The most distinct characteristics of the harmonic spectrum are the numerous *Fermi resonances* (degeneracies) [10,45] that appear at certain values of $\tilde{B}$, some of which we indicate with vertical lines in the figure. These values of $\tilde{B}$ are determined by the Fermi resonance condition $\ell\omega_1=k\omega_2$, where ℓ and k are any two integers [18]. For example, as highlighted in the figure, the $|11\rangle$ and $|05\rangle$ states are degenerate at harmonic order near $\tilde{B}=320$, where the ratio $\omega_1/\omega_2=4$. Therefore, we say that these two states, even at converged orders, are related through a 4:1 Fermi resonance. To determine which states coincide with a given Fermi resonance, consider two states $|ab\rangle$ and $|cd\rangle$. The harmonic energy levels of these two states cross at the $X:Y$

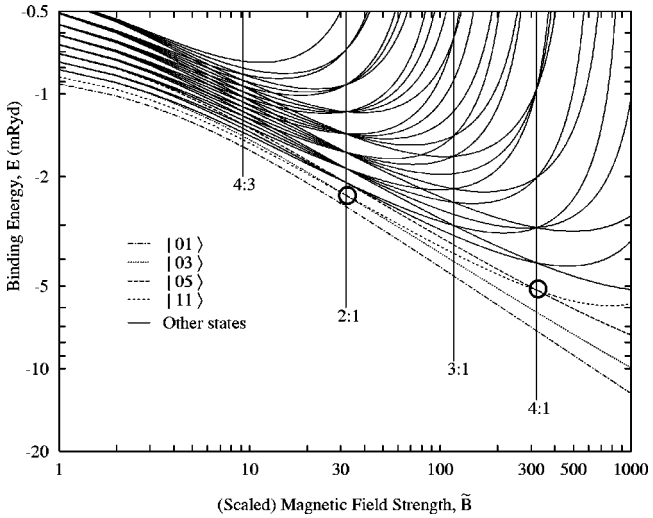

FIG. 2. Harmonic (zeroth-order) energy levels as functions of $\tilde{B}$ for diamagnetic hydrogen. The vertical axis measures binding energy in mRy for $|m|=33$. The vertical lines denote some prominent degeneracies (Fermi resonances) appearing in the spectrum. The crossings explicitly discussed the most in this paper are highlighted in bold circles: one associated with a 4:1 Fermi resonance at $\tilde{B}=320.8$ and the other with a 2:1 Fermi resonance at $\tilde{B}=32.1$. Only levels corresponding to the ten lowest hydrogenic ($\tilde{B}=0$) shells are shown.

Fermi resonance provided $Xa+Yb=Xc+Yd$. For example, the $|15\rangle$ and $|41\rangle$ harmonic levels cross at the 4:3 Fermi resonance, since $4\times1+3\times5=4\times4+3\times1$. We show more examples in Table I. In Fig. 2 we highlight energy-level crossings at two particular Fermi resonances: a 2:1 Fermi resonance ($\omega_1=2\omega_2$) between the $|03\rangle$ and $|11\rangle$ states and a 4:1 Fermi resonance ($\omega_1=4\omega_2$) between the $|05\rangle$ and $|11\rangle$ states. Although the $|11\rangle$ and $|03\rangle$ states are not the only states that interact through a 2:1 Fermi resonance, we will consider only these two states when we discuss this particular Fermi resonance. Along the same lines, we will discuss only the interaction between the $|11\rangle$ and $|05\rangle$ states when we focus on the 4:1 Fermi resonance.

At finite $|m|$, terms in the Hamiltonian that couple the $\hat{\rho}$ and $\hat{z}$ degrees of freedom are no longer negligible. Therefore, level crossings become forbidden by the Wigner–von Neumann noncrossing rule and are replaced by avoided crossings. The avoided crossing center at finite $|m|$ is displaced from the harmonic crossing because of the $|m|$ dependence of the energy levels. As an example, in Fig. 3 the 4:1 crossing highlighted in Fig. 2 is displaced from $\tilde{B}=320.8$ (the harmonic *level* crossing) to $\tilde{B}=138.4$ (the *avoided* crossing). In Fig. 4 we show the avoided crossing in Fig. 3 in more detail, making the character exchange occurring in the vicinity of the avoided crossing easier to see. We can see that the two energy levels do not cross. Despite this shift in location, we can still associate the avoided crossing with the 4:1 Fermi resonance because as $|m|\to\infty$ the avoided crossing location approaches the 4:1 Fermi resonance degeneracy. Therefore, even though the spectrum of diamagnetic hydrogen contains a complex arrangement of avoided crossings, we can use the harmonic energy spectrum to assign each avoided crossing to a particular Fermi resonance.

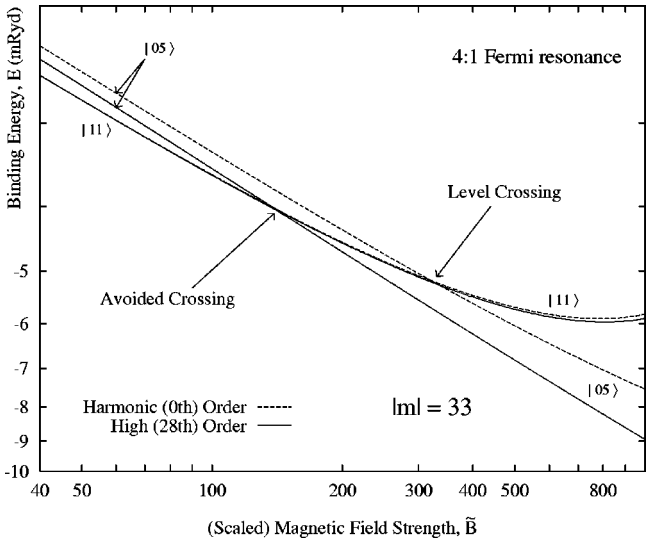

FIG. 3. Harmonic ($p=0$) and convergent ($p=28$) energy levels of the $|m|=33$ $|05\rangle$ and $|11\rangle$ states related to the 4:1 Fermi resonance degeneracy highlighted in Fig. 2. Note the shift of the minimum energy separation to lower $\tilde{B}$ in the convergent spectrum.

We now turn our attention to the avoided crossings that appear between two energy levels when we plot the energy as a function of *angular momentum*. We show that not only is there a clear relationship between the E-versus-B and the E-versus-$|m|$ spectra, but we can understand this relationship by examining the branch points that connect the two energy levels.

V. ENERGY AS A FUNCTION OF ANGULAR MOMENTUM

In Fig. 4 an avoided crossing in the E-versus-$\tilde{B}$ spectrum appeared [46] at $\tilde{B}=138.4$ when the angular momentum was fixed at $|m|=33$. From Eq. (12) this corresponds to B

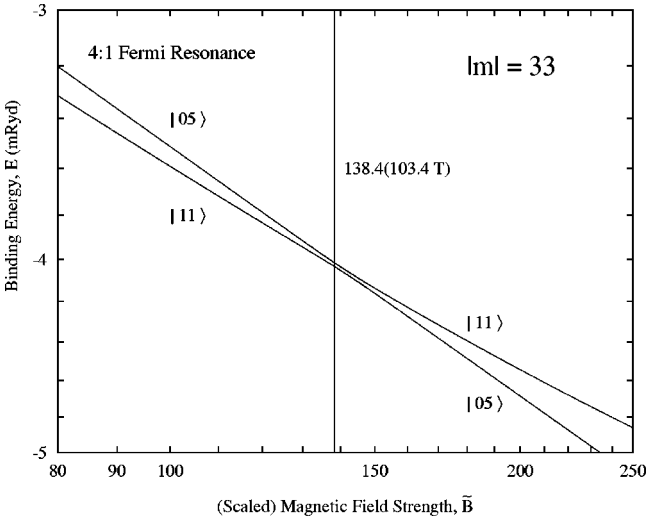

FIG. 4. Detail of the converged ($p=28$) energy levels shown in Fig. 3. The character of the wave function, which is represented by $|\nu_1\nu_2\rangle$, is exchanged diabatically as the magnetic field sweeps past the avoided crossing. Note that the avoided crossing center occurs at $\tilde{B}=138.4$, which is equivalent in this case ($|m|=33$) to $B=103.4$ T (noted in parentheses).

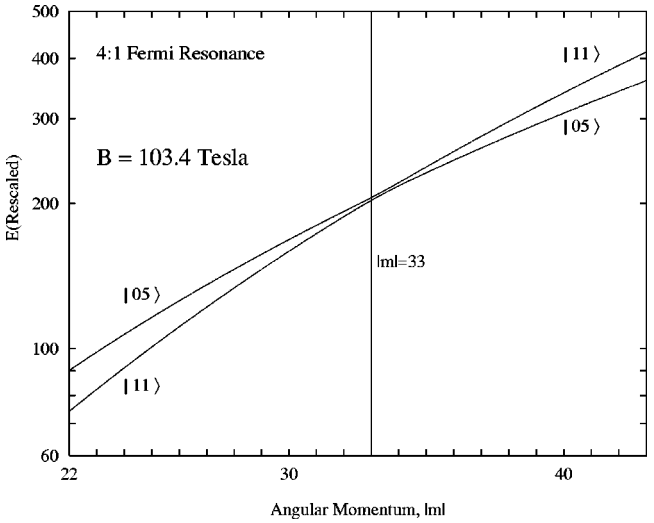

FIG. 5. In contrast to Fig. 4, here we plot E as a function of $|m|$, not $\tilde{B}$, with B held fixed at 103.4 T. Note that the avoided crossing is centered about $|m|=33$ (rounded to the nearest integer). Note the change in scaling for the vertical axis [48].

$=103.4$ T. We now consider $|m|$ as a continuously varying real parameter and see how the system energy responds as B is held fixed at 103.4 T and $|m|$ is changed.

Consider Fig. 5, which shows the same two energy levels for the 4:1 Fermi resonance as $|m|$ is changed. With $B=103.4$ T, the avoided crossing occurs near $|m|=33$, rounded to the nearest integer. Therefore, there is a strong correspondence between avoided crossings appearing in the E-versus-B spectra and those appearing in the E-versus-$|m|$ spectra: If $|m|$ is fixed at $|m|\equiv|m|_0$ while B is swept, an avoided crossing appears at some value $B\equiv B_0$. Correspondingly, if B is fixed at B_0 while $|m|$ is swept, an avoided crossing appears at $|m|_0$. This correlation between the avoided crossings in the E-versus-B and the E-versus-$|m|$ spectra points to the existence of nearby degeneracies that cause an avoided crossing whether we sweep B or $|m|$. We discuss this in detail in the next two sections.

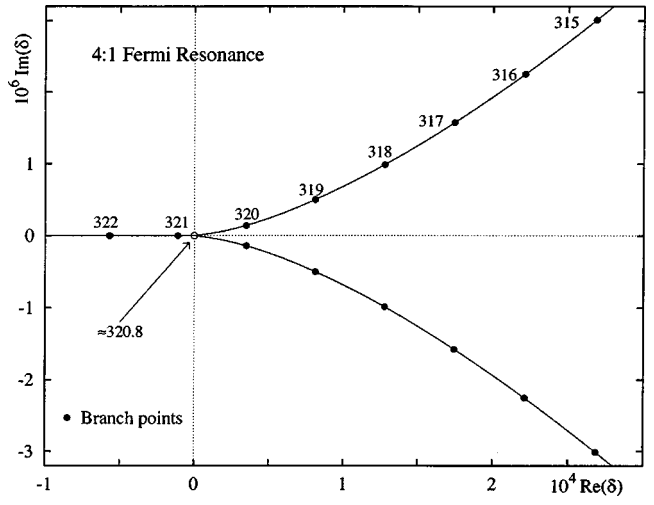

FIG. 6. Branch point structure of diamagnetic hydrogen in the complex-δ plane relating to the 4:1 Fermi resonance involving the $|11\rangle$ and $|05\rangle$ states [49]. The numbers near each branch point refer to the corresponding value of $\tilde{B}$. Note that the locations of the branch points are particular to a given value of $\tilde{B}$ and that they move to the left as $\tilde{B}$ increases. Due to the scaling of the axes, the branch points on the negative real axis appear to be located at the same point. They are, however, separated and this separation increases for increasing $\tilde{B}$.

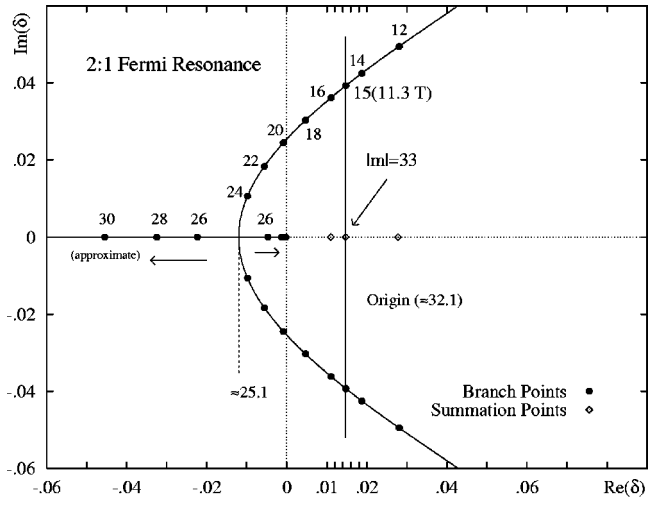

FIG. 7. Branch point structure of diamagnetic hydrogen relating to a 2:1 Fermi resonance involving the $|11\rangle$ and $|03\rangle$ state for field strengths up to $\tilde{B}=30$. As in Fig. 6 the numbers by each branch point refer to $\tilde{B}$. The number in the parentheses refers to the corresponding value of B in tesla for $|m|=33$ and $D=3$. The arrows on the real axis indicate the direction the branch points move with increasing magnetic-field strength. The arrow closest to the origin will reverse direction once that branch point reaches the origin (at $\tilde{B}\approx 32.1$). The unmarked branch points close to the origin correspond to (from left to right) $\tilde{B}=28$ and $\tilde{B}=30$. The summation points correspond to (from left to right) $|m|=44$, $|m|=33$, and $|m|=17$ and are referenced in Table III. The vertical line at $|m|=33$ is referenced in the text.

VI. ENERGY-LEVEL CHARACTERIZATION AND AVOIDED CROSSINGS

In [36] we argue that the behavior of the branch points as functions of $\tilde{B}$ for both the 4:1 and 2:1 Fermi resonances indicates that the energy levels of a two-state Fermi resonance have the analytic form

$$E_{\pm}(\delta,\tilde{B})=\tilde{E}_a(\delta,\tilde{B})\pm\tilde{E}_b(\delta,\tilde{B})\sqrt{\delta-\tilde{\delta}_+(\tilde{B})}\sqrt{\delta-\tilde{\delta}_-(\tilde{B})}. \tag{25}$$

For the rest of this discussion we must keep in mind that the summation point δ is directly related to $|m|$ in three dimensions through the relation $\delta=1/(2+2|m|)$. The branch point locations $\tilde{\delta}_+(\tilde{B})$ and $\tilde{\delta}_-(\tilde{B})$ are solutions of the equation

$$\Delta E(\delta,\tilde{B})\equiv E_+(\delta,\tilde{B})-E_-(\delta,\tilde{B})$$
$$=2E_b(\delta,\tilde{B})\sqrt{\delta-\tilde{\delta}(\tilde{B})}\sqrt{\delta-\tilde{\delta}(\tilde{B})}=0 \tag{26}$$

for fixed $\tilde{B}$. (See Sec. II.)

The branch point trajectories in the complex-δ plane are shown for a 4:1 and a 2:1 Fermi resonance in Figs. 6 and 7,

respectively. Notice that the branch points for the 4:1 Fermi resonance in Fig. 6 are initially complex conjugate and approach the origin as $\tilde{B}$ increases towards the value $\tilde{B}=320.8$. (This is the same value of $\tilde{B}$ that corresponds to the 4:1 Fermi resonance.) As $\tilde{B}$ increases beyond this value the branch points form on the negative real axis and head towards $-\infty$, although at slightly different rates.

The branch point structure of the 2:1 Fermi resonance in Fig. 7 looks more complicated. Here the branch points are complex conjugate until $\tilde{B}\approx 25.1$, at which point they coalesce onto the negative real axis. As $\tilde{B}$ further increases one of the branch points will head towards $-\infty$ while the other will head towards the origin, reaching that point at $\tilde{B}\approx 32.1$. (This value of $\tilde{B}$ corresponds to the 2:1 Fermi resonance.) From there the latter branch point reverses direction and both branch points will then be moving towards $-\infty$.

As required, when δ equals either $\tilde{\delta}_+(\tilde{B})$ or $\tilde{\delta}_-(\tilde{B})$ the energies E_+ and E_- become equal (degenerate). Note that $\tilde{\delta}_-=(\tilde{\delta}_+)^*$ unless the branch points lie on the real axis (again, a consequence of the Schwarz reflection principle). Thus, when δ lies on the real axis (the physically relevant situation) and the branch points lie off the real axis in the complex plane. The summation point δ is symmetrically placed between the complex-conjugate pair of branch points and the term $\sqrt{\delta-\tilde{\delta}_+(\tilde{B})}\sqrt{\delta-\tilde{\delta}_-(\tilde{B})}$ in Eq. (25) is just the distance in the complex plane from the point δ to either of the two branch points.

In Sec. II we argued that avoided crossings will occur close to complex-conjugate square-root branch point degeneracies present in the complex parameter plane. In this section we use the energy-level characterization in Eq. (25) to sharpen our understanding of the relationship between the locations of avoided crossings and the branch point structure of diamagnetic hydrogen. First we consider in Sec. VI A 1 avoided crossings as $|m|$ is swept while the magnetic-field strength is fixed. Dimensional perturbation theory is naturally formulated in terms of the scaled field strength $\tilde{B}$ and so automatically provides results for fixed $\tilde{B}$. From an experimental point of view, investigating the response of the system to changes in $|m|$ for fixed $\tilde{B}$ would appear to be quite feasible, although obviously $|m|$ is limited to integer values. As $|m|$ is changed, the unscaled field strength will have to be appropriately altered [see Eq. (12)]. In Sec. VI A 2 we also consider the case of avoided crossings as $|m|$ is swept while the *unscaled* field strength B is held constant.

A. The 4:1 Fermi resonance: Avoided crossings as $|m|$ is swept

1. Scaled field strengths held constant

We define the center of the avoided crossing ${}^{\rm AC}\tilde{\delta}(\tilde{B})$ to be the value of δ where ΔE is a minimum. While there is no reason to believe that the $\tilde{E}_b$ term in Eq. (25) should remain constant over any appreciable range of angular momentum or magnetic-field strengths, the avoided crossing for the 4:1 Fermi resonance is so sharp in both spectra that we can expect $\tilde{E}_b$ not to vary significantly from one side of the avoided crossing to the other. (We will see that this assumption fails for the broad avoided crossings of the 2:1 Fermi resonance.) Therefore, the center of the avoided crossing occurs when the distance from the summation point δ to the branch points is a minimum, that is

$$ {}^{\rm AC}\tilde{\delta}(\tilde{B})=\mathrm{Re}[\tilde{\delta}_{\pm}(\tilde{B})]. \tag{27}$$

Therefore, as long as the branch point is held fixed ($\tilde{B}$ is held fixed) and $|m|$ is swept, we can make the following assertion: *Since $\tilde{E}_b$ is roughly constant over the avoided crossing region, the avoided crossing appears whenever the summation point δ reaches the vicinity of ${}^{\rm AC}\delta(\tilde{B})$, the real component of the branch point locations on the complex-δ plane.*

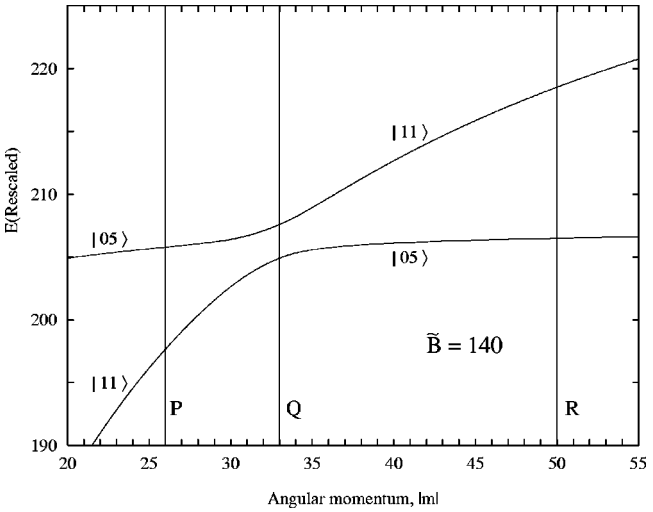

FIG. 8. Energy as a function of angular momentum for the 4:1 Fermi resonance. Here, instead of fixing B as in Fig. 5, we fix $\tilde{B}$. As in Fig. 5 we rescaled the vertical axis.

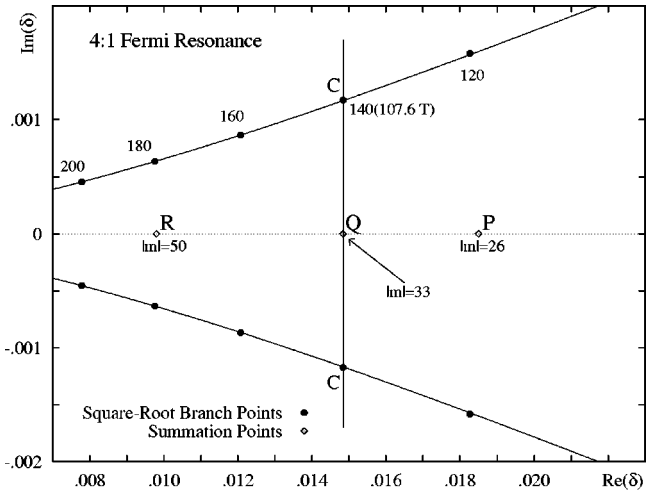

FIG. 9. Another view of the data in Fig. 6, the branch point structure of the 4:1 Fermi resonance, plotted at lower values of $\tilde{B}$. The values of $|m|$ shown correspond to $D=3$ and are referenced in Table II and the text. The numbers near each branch point refer to the corresponding values of $\tilde{B}$. The number in parentheses refers to the magnetic-field strength B in tesla for $|m|=33$. The vertical line at $|m|=33$ is referred to in the text.

TABLE II. Avoided crossing locations in the E-versus-B spectrum for the 4:1 Fermi resonance. The summation points corresponding to $|m|=26$, 33, and 50 are illustrated in Fig. 9. The $\mathrm{Re}(\delta^{\pm})$ that corresponds to each $|m|$ assumes $D=3$.

4:1 Fermi resonance					
$\lvert m\rvert$	$\mathrm{Re}(\delta^{\pm})$	$\tilde{B}^{a}$	B (T)^{a}	$\tilde{B}^{b}$	B (T)^{b}
26	0.019	120	179	116.7	174.1
33	0.015	140	105	138.4	103.4
50	0.010	180	40	180.0	39.9

[a]Predicted value from scanning Fig. 6.
[b]Computed value from Padé summing Eq. (17) for the two energy levels (see [47]).

We now use this result to predict the locations of avoided crossings appearing in the E-versus-$|m|$ spectrum. In Fig. 8 the energy levels of the $|11\rangle$ and $|05\rangle$ states are plotted as functions of $|m|$, but this time for fixed $\tilde{B}$, not B. Now consider the summation point P in Fig. 9, which corresponds to $|m|=26$ in three dimensions. (Figure 9 is the same as Fig. 6, but for lower values of $\tilde{B}$.) If we sum the energy series about this point, we determine the resulting energies by referring to the energy levels in Fig. 8 that intersect line P. In fact, with the use of Eq. (27) we can understand the entire dependence of E on $|m|$ by fixing $\tilde{B}$ and sweeping the summation point δ (therefore sweeping $|m|$) along the real axis in the complex-δ plane. For example, suppose we fix $\tilde{B}=140$, therefore fixing the branch point locations at points C in Fig. 9, and sweep $|m|$ from point P to point R. An avoided crossing occurs when we reach point Q because at that point $\mathrm{Re}(\tilde{\delta}_{\pm})$ coincides with the summation point δ. We can verify this result by referring to Fig. 8.

2. Unscaled field strengths held constant

As stated earlier, the locations on the complex-δ plane of the branch points that connect the two energy levels are purely functions of $\tilde{B}$. However, since the relationship between $\tilde{B}$ and B in Eq. (12) involves $|m|$, the branch points cannot be fixed in location in the complex δ plane while $|m|$ (that is, δ) is swept with B constant.

However, it turns out that Eq. (27) also applies when the *unscaled* field strength B is held fixed, with $\tilde{B}$ replaced by B in the equation. To see this, Eq. (25) needs to be reexpressed in terms of B (rather than $\tilde{B}$) and the solutions $\delta_{\pm}(B)$ of the equation

$$\Delta E(\delta,B)=0 \tag{28}$$

calculated for fixed B [rather than $\tilde{\delta}_{\pm}(\tilde{B})$, the solutions of Eq. (26) for fixed $\tilde{B}$]. This is done in Sec. 1 of the Appendix with the result

$$E_{\pm}(\delta,B)=E_a(\delta,B)\pm E_b(\delta,B)\sqrt{\delta-\delta_+(B)}\sqrt{\delta-\delta_-(B)}. \tag{29}$$

Compare this with Eq. (25). Analogously to Eq. (25), when δ lies on the real axis and the branch points lie off the real axis in the complex plane, the term $\sqrt{\delta-\delta_+(B)}\sqrt{\delta-\delta_-(B)}$ in Eq. (29) is just the distance in the complex plane from the point δ to either of the two branch points with B held fixed.

Thus assuming that $E_b(\delta,B)$ in Eq. (29) is constant under changes in $|m|$ throughout the region spanning the avoided crossing, then the center of the avoided crossing occurs when the distance from the point δ to the branch points $\delta_{\pm}(B)$ is a minimum, that is,

$$^{\mathrm{AC}}\delta(B)=\mathrm{Re}[\,\delta_{\pm}(B)\,]. \tag{30}$$

Therefore, as long as the branch point is held fixed (B is held fixed) and $|m|$ is swept, we can make the following assertion: If E_b is roughly constant, the avoided crossing appears whenever the summation point δ reaches the vicinity of $^{\mathrm{AC}}\delta(B)$, the real component of the branch point locations on the complex-δ plane. [See Eq. (27).]

A good approximation for $\mathrm{Re}[\delta_{\pm}(B)]$, the real part of the solutions of Eq. (28) for fixed B, may be obtained from the positions of the branch points in the complex plane for fixed $\tilde{B}$, the solutions $\tilde{\delta}_{\pm}(\tilde{B})$ of Eq. (26). In Sec. 2 of the Appendix we show that since $|\mathrm{Re}[\tilde{\delta}_{\pm}(\tilde{B})]|\gg|\mathrm{Im}[\tilde{\delta}_{\pm}(\tilde{B})]|$, Eq. (30) implies the approximate relationship

$$^{\mathrm{AC}}\delta(\{\mathrm{Re}[\,\tilde{\delta}_{\pm}(\tilde{B})]\}^3\tilde{B})\approx\mathrm{Re}[\,\tilde{\delta}_{\pm}(\tilde{B})]. \tag{31}$$

Therefore, we can predict the locations of avoided crossings in the E-versus-$|m|$ spectrum for fixed B by merely glancing at the branch point structure connecting the two energy levels in the complex-δ plane for fixed $\tilde{B}$. For example, in Fig. 9 we see that the real part of the branch point locations corresponding to $\tilde{B}=140$ is at roughly the same location as the summation point corresponding to $|m|=33$. At these values of $|m|$ and $\tilde{B}$, the physical field strength is $B=107.6$ T. Therefore, we would expect an avoided crossing to appear at $B=107.6$ T when $|m|$ is fixed at 33. This is close to where the avoided crossing appears in Fig. 5, at $B=103.4$ T.

Next we consider avoided crossings as the magnetic-field strength, either scaled or unscaled, is swept while $|m|$ is unchanged.

B. The 4:1 Fermi resonance: Avoided crossings as the magnetic-field strength is swept

Let us hold $|m|$ (or equivalently δ) constant on the real line and sweep $\tilde{B}$. An avoided crossing appears at that value of $\tilde{B}$ for which $\Delta E(\delta,\tilde{B})$ is a minimum. Suppose $\tilde{E}_b$ in Eq. (25) is constant under changes in $\tilde{B}$ throughout the region spanning the avoided crossing. Thus, from Eq. (25) the avoided crossing occurs when the branch point trajectories in the complex plane pass closest to the summation point δ.

By examining the horizontal and vertical scaling in Figs. 6 and 9 we see that the gradient of the branch point trajectories remains quite small and so to a good approximation the point of closest approach occurs when

$$\mathrm{Re}[\,\tilde{\delta}_{\pm}(\tilde{B})]=\delta. \tag{32}$$

Therefore, if $\tilde{E}_b$ is roughly constant over the avoided crossing and the slope of the branch point trajectories to the real

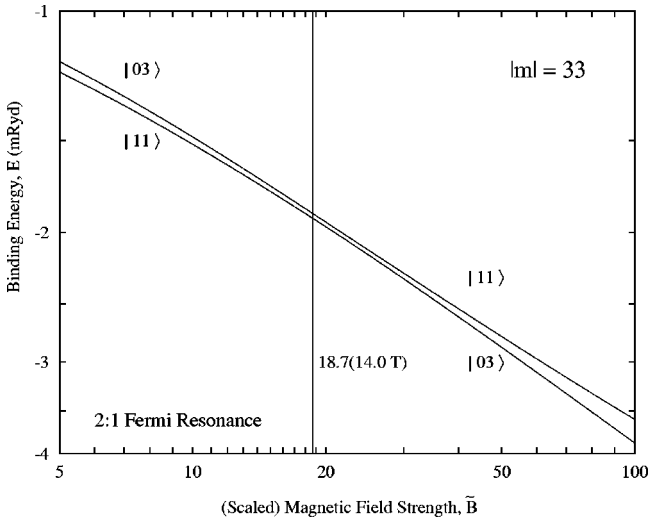

FIG. 10. Detail of the interaction between the $|03\rangle$ and $|11\rangle$ states associated with a 2:1 Fermi resonance. As in Fig. 4 the number in parentheses refers to the magnetic-field strength in tesla when $|m|=33$.

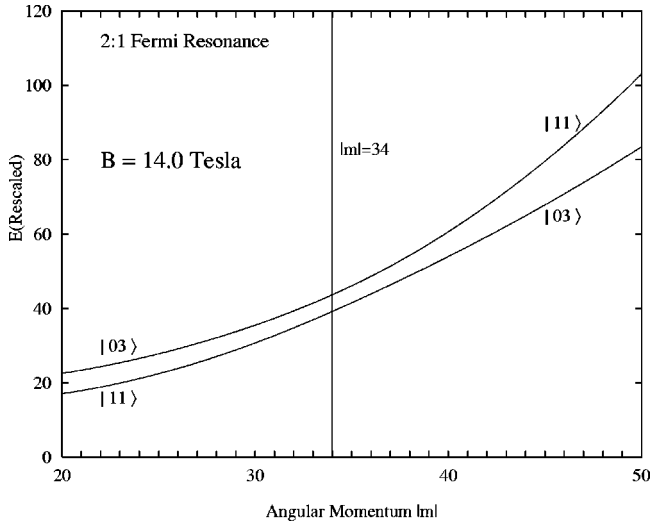

FIG. 11. Same as Fig. 5 except for a 2:1 Fermi resonance. Here we fix $B=14.0$ T. The avoided crossing here is close to $|m|=34$, rounded to the nearest integer. As in Fig. 5 we rescaled the vertical axis.

line is small, i.e., $|\mathrm{Re}[\tilde{\delta}_{\pm}(\tilde{B})]| \gg |\mathrm{Im}[\tilde{\delta}_{\pm}(\tilde{B})]|$, when the real part of the branch points $\mathrm{Re}[\tilde{\delta}_{\pm}(\tilde{B})]$ reaches the summation point δ, the separation between the two energy levels is close to a minimum. To a good approximation we can say that the center of the avoided crossing has been reached. For example, if we fix $|m|=33$ (point Q in Fig. 9) and sweep $\tilde{B}$, we should get an avoided crossing near $\tilde{B}=140$. The crossing actually occurs at $\tilde{B}=138.7$, as we saw in Fig. 4. As seen in Eq. (11), any result for which $|m|$ is held fixed equally applies to either sweeping $\tilde{B}$ or B since B and $\tilde{B}$ are then directly proportional.

In Table II we predict the locations of avoided crossings for both scaled and physical magnetic-field strengths for three different fixed values of $|m|$. From this table we see that the branch point structure of the 4:1 Fermi resonance provides a convenient way of accurately determining such avoided crossing locations. In conclusion, it is possible to predict the locations of avoided crossings in the E-versus-$|m|$ spectrum for fixed B (or $\tilde{B}$) and the E-versus-$\tilde{B}$ (or B) spectra for fixed $|m|$ by merely glancing at the branch point structure connecting the two energy levels in the complex-δ plane for fixed $\tilde{B}$.

VII. THE 2:1 FERMI RESONANCE

Having established the relationship between avoided crossings and branch point structure by focusing on the 4:1 Fermi resonance, we now direct our attention to the 2:1 Fermi resonance. By examining Figs. 10 and 11 we can see that the same correspondence between the two spectra that exists for the 4:1 Fermi resonance applies to the 2:1 Fermi resonance as well. (i) An avoided crossing appears at $B=14.0$ T for $|m|$ fixed at $|m|=33$. (ii) With B fixed at $B=14.0$ T an avoided crossing appears at $|m|=34$. Notice that since the avoided crossing appears at $|m|=34$ and not $|m|=33$, the correspondence between the two plots is not as precise as it was for the 4:1 Fermi resonance. We will discuss this further below.

The repulsion between the $|11\rangle$ and $|03\rangle$ states is quite strong [36], therefore the avoided crossing is actually spread out over a large region of magnetic-field strength. Therefore, we should not expect $\tilde{E}_b$ in Eq. (25) to remain nearly constant throughout the avoided crossing region. However, our previous discussion relied on a roughly constant $\tilde{E}_b$, so we now see how our results apply to the 2:1 Fermi resonance.

A. Avoided crossings as $|m|$ is swept

1. Scaled field strengths held constant

In Fig. 12 energy is plotted as a function of $|m|$, with the scaled magnetic-field strength fixed to $\tilde{B}=15$. According to the argument in Sec. VI, an avoided crossing should appear when the summation point reaches the real part of the branch points corresponding to $\tilde{B}=15$. According to Fig. 7, this should be near $|m|=33$ (note the vertical line that runs through the $|m|=33$ summation point and the branch point corresponding to $\tilde{B}=15$). However, Fig. 12 shows that the avoided crossing appears at $|m|=19.0$. The only approximation that went into Eq. (27) was that $\tilde{E}_b$ was nearly constant, so at this point we can conclude that for the 2:1 Fermi resonance $\tilde{E}_b$ changes significantly over the region of the avoided crossing. This means that the first term

$$\frac{\partial(\Delta E)}{\partial\delta}=2\frac{\partial\tilde{E}_b}{\partial\delta}\sqrt{\delta^2-(\delta_+ +\delta_-)\delta+\delta_+\delta_-} + \frac{\tilde{E}_b[2\delta-(\delta_+ +\delta_-)]}{\sqrt{\delta^2-(\delta_+ +\delta_-)\delta+\delta_+\delta_-}} \tag{33}$$

in the derivative of Eq. (26) is appreciable in comparison to the second.

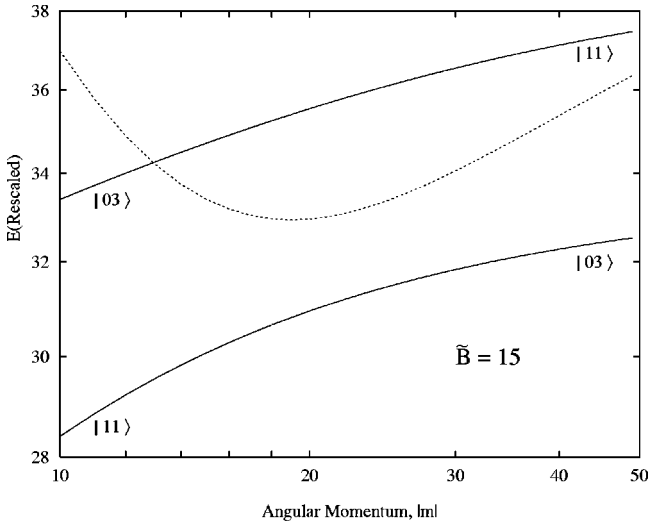

FIG. 12. Energy levels corresponding to a 2:1 Fermi resonance as $|m|$ is swept. Here we hold the scaled magnetic field $\tilde{B}$ fixed. The dashed line is the difference between the two energies, scaled to fit on the same plot. The minimum (avoided crossing) occurs at $|m| = 19.0$. All energies have been rescaled.

For $\tilde{B}=15$ the fact that $\tilde{E}_b$ varies significantly over the avoided crossing region is easily shown. From a plot of $\tilde{E}_b$ as a function of δ (that is, $|m|$) over the avoided crossing region (see Fig. 13) we see that $\tilde{E}_b$ roughly has the form

$$\tilde{E}_b = -C_1\delta + C_2, \tag{34}$$

where $C_1 \approx 344$ and $C_2 \approx 65.3$. Substituting this expression into Eq. (33) and noting that $\delta_{\pm} \approx 0.0147 \pm 0.0393$ for $\tilde{B} = 15$, we find that the ratio of the first term to the second term in Eq. (33) lies roughly anywhere between 0.25 and 1.0 from one end of the avoided crossing to the other. Therefore,

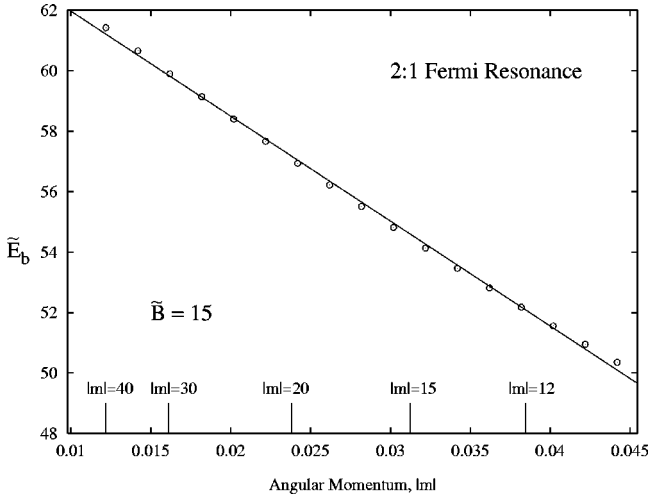

FIG. 13. The $\tilde{E}_b$ term in Eq. (25) plotted as a function of δ over the range of the avoided crossing in Fig. 12. The corresponding values of $|m|$ are shown for reference ($D=3$). The extreme left of the plot corresponds to $|m|=50$, whereas the extreme right corresponds to $|m|=10$.

the first term in Eq. (33) containing $\partial\tilde{E}_b/\partial\delta$ cannot be ignored, so $\tilde{E}_b$ is not sufficiently constant throughout the avoided crossing region.

With the linear approximation of Eq. (34), from Eq. (33) $\partial(\Delta E)/\partial\delta = 0$ places the avoided crossing center at $|m| \approx 19.3$, which is very close to the exact value of $|m| = 19.0$ (see Fig. 12). Therefore, by merely taking into account the next term of the Taylor series expansion of $\tilde{E}_b$ with respect to δ, we accurately obtain the position of the avoided crossing at the 2:1 Fermi resonance.

2. Unscaled field strengths held constant

In Sec. VI A 2 we found that the same relationship for predicting the appearance of avoided crossings for fixed *scaled* field strength also applied to fixed *unscaled* field strength because the approximation $|\mathrm{Re}[\tilde{\delta}_{\pm}(\tilde{B})]| \gg |\mathrm{Im}[\tilde{\delta}_{\pm}(\tilde{B})]|$ applied. In Fig. 7 we can see that such an approximation does not apply to the 2:1 Fermi resonance.

B. Avoided crossings as the magnetic-field strength is swept

When sweeping the magnetic-field strength (scaled or unscaled) for the 4:1 Fermi resonance we simplified the predictions of avoided crossings by noting that the trajectories of the branch points were nearly parallel to the real axis. Therefore, for the 4:1 interaction the closest distance between the branch point and the summation point simply coincided with the summation point located at the real part of the branch point. A glance at Fig. 7 shows that this simplification will not hold for the 2:1 Fermi resonance. However, finding the branch point that is closest to the summation point from a plot of the branch point trajectory is not too difficult as long as the real and imaginary axes are scaled the same, as in the figure. Here we can see that for $|m|=33$ the branch point coinciding with $\tilde{B} \approx 23$ is closest to the summation point, so we expect to find an avoided crossing at roughly $\tilde{B}=23$ if we fix $|m|=33$. However, Fig. 10 shows that the avoided cross-

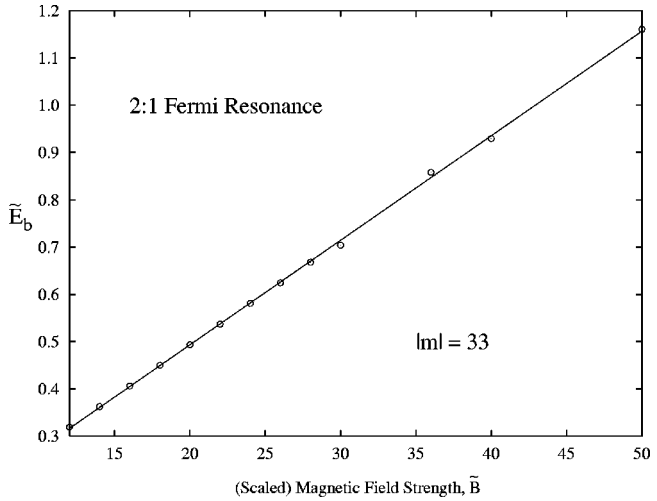

FIG. 14. The $\tilde{E}_b$ term in Eq. (25) plotted as a function of $\tilde{B}$ over the range of the avoided crossing in Fig. 10. Clearly $\tilde{E}_b$ is not constant over this range of field strengths.

TABLE III. Avoided crossing locations in the E-versus-B spectrum for the 2:1 Fermi resonance. The summation points corresponding to $|m|=17$, 33, and 44 are illustrated in Fig. 7. The $\mathrm{Re}(\delta^{\pm})$ that corresponds to each $|m|$ assumes $D=3$.

2:1 Fermi resonance					
$\lvert m\rvert$	$\mathrm{Re}(\delta^{\pm})$	$\tilde{B}^{a}$	$B(\mathrm{T})^{a}$	$\tilde{B}^{b}$	$B(\mathrm{T})^{b}$
17	0.028	19	96	13.0	65.5
33	0.015	23	17	18.7	14.0
44	0.011	25	8	21.6	7.0

[a]Predicted value from visually scanning Fig. 7.
[b]Computed value from Padé summing Eq. (17) for the two energy levels.

ing actually appears at $\tilde{B}=18.7$. By plotting $\tilde{E}_b$ as a function of $\tilde{B}$ in Fig. 14 and noting that $\tilde{E}_b$ increases by roughly a factor of 4 over the range of the avoided crossing, we can verify that $\tilde{E}_b$ varies considerably over the region of the avoided crossing for this interaction, so such a discrepancy is not unexpected.

Just as for the 4:1 Fermi resonance between the $|11\rangle$ and $|05\rangle$ states, we summarize in Table III comparisons between expected and calculated results corresponding to those summation points shown in Fig. 7, the branch point structure of the 2:1 Fermi resonance between the $|11\rangle$ and $|03\rangle$ states. Despite the discrepancy in assuming a constant $\tilde{E}_b$, the predicted values are still fairly close to those found by computer calculation for a wide range of $|m|$.

VIII. EVEN-PARITY STATES

All calculations in this paper focused on odd-parity states. However, even-parity energy levels and branch point trajectories are essentially the same as for odd-parity states. As examples we show the *even-parity* branch point structure of 4:1 and 2:1 Fermi resonances in Figs. 15 and 16. Comparing these figures to Figs. 6 and 7 it appears that, except for slight shifts in locations, the branch point structures are essentially the same. Therefore, the energy-level characterization in Eq. (25) applies to both even- and odd-parity states.

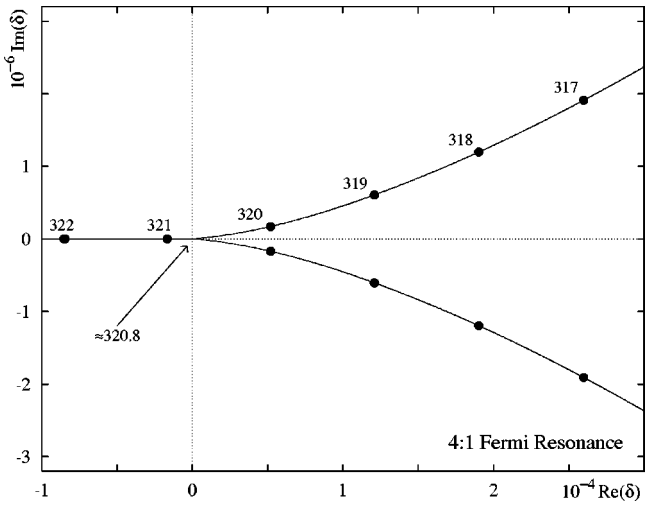

FIG. 15. Same as Fig. 6 except this time we show the *even-parity* branch point structure involving the $|10\rangle$ and $|04\rangle$ states.

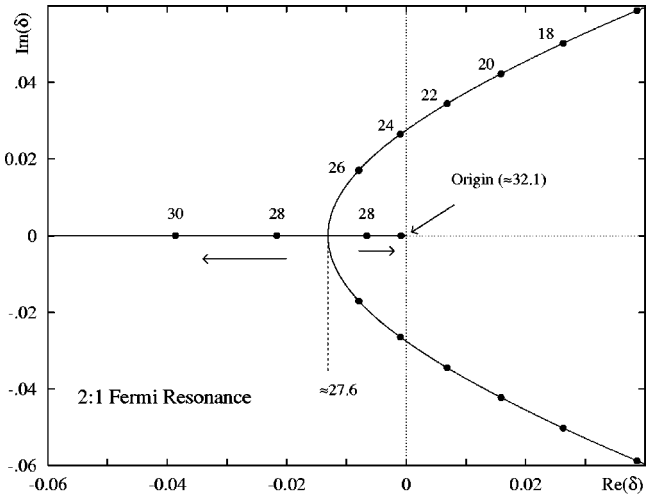

FIG. 16. Same as Fig. 7, except this time we show the *even-parity* branch point structure involving the $|10\rangle$ and $|02\rangle$ states. The branch points close to the origin and lying on the negative real axis correspond to (from left to right) $\tilde{B}=28$ and $\tilde{B}=30$.

This is not surprising since dimensional perturbation theory shows that at harmonic order the location of the Fermi resonances, which determines the location of degeneracy at higher order and thus the location of branch points, is the same for either parity. (Watson *et al.* [29] include a plot of the harmonic-order even-parity energy levels as a function of $\tilde{B}$, although at a different value of $|m|$.) Because of this similarity in the harmonic-order spectra between the two parities, the even-parity energy levels share the same qualitative features as their odd-parity counterparts. Some examples of even-parity counterparts to the odd-parity E-versus-B spectra are shown by Watson *et al.*, again for a different value of $|m|$.

IX. CONCLUSIONS AND SUMMARY

In this paper we examined two types of spectra. In one the angular momentum $|m|$ was held constant while the *magnetic field B* changed adiabatically and in the other the magnetic field was held constant while the *angular momentum* changed adiabatically. We found that the locations of the avoided crossings appearing in the E-versus-B spectra are directly related to the locations of those appearing in the E-versus-$|m|$ spectra and that this correspondence points to a degeneracy in the energy levels that provides the mechanism for the appearance of avoided crossings in both spectra.

The branch points that connect the energy levels are the mathematical basis of such a mechanism [51] and by understanding this basis we have found it possible to predict the locations of avoided crossings in both spectra. By successfully characterizing the energy levels in terms of these branch points through Eq. (25), a simple relationship that merely requires visually examining the branch point trajectories of the system as functions of B was found that could be used for predicting the locations of avoided crossings in both spectra.

Although we have only explicitly analyzed the situation

involving two strongly interacting states (two-state Fermi resonances), Table I shows that three and more strongly interacting states (three- and more-state Fermi resonances) are common in the eigenvalue spectrum of diamagnetic hydrogen. Heiss and Steeb [52] have studied the analytic characterization of branch points of the eigenvalues associated with avoided crossings of three and more strongly interacting states in finite-dimensional matrix eigenvalue problems. They find that in this case Eq. (25) correctly characterizes the branch point structure of the eigenvalues in the neighborhoods of the branch points. Thus, although infinite-dimensional matrix equations can in principle involve more complex branch point characterizations [36] involving states with complex energies (resonances) [53], we expect that Eq. (25) will still correctly parametrize the energy involving three and more strongly interacting states in the neighborhood of branch points that will produce avoided crossings. Therefore, the analysis performed in this paper should apply to all avoided crossings of diamagnetic hydrogen.

The ability to predict and understand the appearance of avoided crossings is aided by the assumption that the $\tilde{E}_b$ term in Eq. (25) is constant over the range of the avoided crossing. The avoided crossing pertaining to the 4:1 Fermi resonance was sufficiently sharp to satisfy this assumption, but we saw that because of the broad avoided crossing in the 2:1 Fermi resonance this condition failed. Therefore, predicting the positions of the avoided crossings for the 2:1 Fermi resonance is more involved. However, the broadness of the 2:1 Fermi resonance is the exception rather than the rule [50]. Therefore, the ability to predict the locations of avoided crossings based only on examining the positions of the branch points that connect the two levels should have broad applicability throughout the spectra of diamagnetic hydrogen.

ACKNOWLEDGMENTS

This work was supported by a grant from the Office of Naval Research (Grant No. N000014-94-1-0998). The work at LANL was carried out under the auspices of the U.S. Department of Energy.

APPENDIX: DETAILS OF AVOIDED CROSSINGS AS $|m|$ IS SWEPT WHILE THE UNSCALED FIELD STRENGTH B IS HELD CONSTANT

1. Rewriting the energy-level characterization of Eqs. (25) and (26) in terms of the unscaled field strength and the solutions of Eq. (26) for fixed B

When reexpressed in terms of B and δ, the $\tilde{\delta}_{\pm}(\tilde{B})$ of Eqs. (25) and (26) are functions of both B *and* δ [see Eq. (11)], that is, $\tilde{\delta}_{\pm}(B,\delta)$. Consider expanding $\tilde{\delta}_{\pm}(B,\delta)$ about a point δ_c while B is held fixed, where δ_c is a solution of Eq. (28) for fixed B. Then

$$\tilde{\delta}_{\pm}(B,\delta)=\tilde{\delta}_{\pm}(B,\delta_c)+\left.\frac{d\tilde{\delta}_{\pm}(B,\delta)}{d\delta}\right|_{\delta=\delta_c}(\delta-\delta_c)$$
$$+(\text{higher order terms in } \delta-\delta_c). \quad \text{(A1)}$$

Now $\tilde{\delta}_{\pm}(B,\delta_c)=\tilde{\delta}_{\pm}(\tilde{B}_c)$ is the solution of $\Delta E(\delta,\tilde{B}_c)=0=\Delta E(\delta,B)$ [see Eqs. (26) and (28)], that is, $\tilde{\delta}_{\pm}(B,\delta_c)=\delta_c$, where $c=\pm$. Therefore,

$$\tilde{\delta}_{\pm}(B,\delta)=\delta_{\pm}+\left.\frac{d\tilde{\delta}_{\pm}(B,\delta)}{d\delta}\right|_{\delta=\delta_c}(\delta-\delta_{\pm})$$
$$+(\text{higher order terms in } \delta-\delta_{\pm}). \quad \text{(A2)}$$

This means that

$$\sqrt{\delta-\tilde{\delta}_{\pm}(\tilde{B})}=\sqrt{A(B,\delta)[\,\delta-\delta_{\pm}(B)]}, \quad \text{(A3)}$$

where $A(B,\delta)$ is finite at $\delta=\delta_{\pm}(B)$, and Eq. (25) becomes

$$E_{\pm}(\delta,B)=E_a(\delta,B)\pm E_b(\delta,B)\sqrt{\delta-\delta_+(B)}\sqrt{\delta-\delta_-(B)}$$

[see, for example, Eq. (25)], where the $\delta_{\pm}(B)$ are solutions of Eq. (28).

2. Derivation of the approximate relationship of Eq. (31) from Eq. (28)

A good approximation for $\mathrm{Re}[\delta_{\pm}(B)]$, the real part of the solutions of Eq. (28) for fixed B, may be obtained from the positions of the branch points in the complex plane for fixed $\tilde{B}$, the solutions $\tilde{\delta}_{\pm}(\tilde{B})$ of Eq. (26). Equation (27) determines where an avoided crossing will be found as $\tilde{B}$ is held fixed. According to Eq. (11), this corresponds to an unscaled magnetic field $B=\{\mathrm{Re}[\tilde{\delta}_{\pm}(\tilde{B})]\}^3\tilde{B}$. By using this value of B in Eq. (28) we obtain the positions of the branch points in the complex-δ plane for this value of B. Therefore, from Eq. (30) we obtain the position of the avoided crossings as B is held to this value. However, the value of B at $\tilde{\delta}_{\pm}(\tilde{B})$, the branch point position with $\tilde{B}$ held fixed, is not $\{\mathrm{Re}[\tilde{\delta}_{\pm}(\tilde{B})]\}^3\tilde{B}$ but rather $[\tilde{\delta}_{\pm}(\tilde{B})]^3\tilde{B}$. Thus the $\tilde{\delta}_{\pm}(\tilde{B})$ are the solutions of Eq. (28) with $B=[\tilde{\delta}_{\pm}(\tilde{B})]^3\tilde{B}$. Nevertheless, these are close to $\{\mathrm{Re}[\tilde{\delta}_{\pm}(\tilde{B})]\}^3\tilde{B}$ since $|\mathrm{Re}[\tilde{\delta}_{\pm}(\tilde{B})]|\gg|\mathrm{Im}[\tilde{\delta}_{\pm}(\tilde{B})]|$. Therefore, assuming that the solutions of Eq. (28) are not extremely sensitive to the precise value of B,

$$\delta_{\pm}(\{\mathrm{Re}[\tilde{\delta}_{\pm}(\tilde{B})]\}^3\tilde{B})\approx\tilde{\delta}_{\pm}(\tilde{B}). \quad \text{(A4)}$$

Therefore, from Eq. (30)

$${}^{\mathrm{AC}}\delta_c(\{\mathrm{Re}[\tilde{\delta}_{\pm}(\tilde{B})]\}^3\tilde{B})\approx\mathrm{Re}[\tilde{\delta}_{\pm}(\tilde{B})].$$

[1] R. H. Garstang, Rep. Prog. Phys. **40**, 105 (1977), and references therein.

[2] D. Delande and J. C. Gay, Phys. Rev. Lett. **66**, 3237 (1991); J. C. Gay, *ibid.* **66**, 145 (1991); W. M. Rösner, G. Wunner, H. Herold, and H. Ruder, J. Phys. B **17**, 29 (1984); D. Wintgen and H. Friedrich, Phys. Rev. A **36**, 131 (1987).

[3] D. Delande and J. C. Gay, Comments At. Mol. Phys. **19**, 35 (1986).

[4] C. Iu, G. R. Welch, M. M. Kash, D. Kleppner, D. Delande, and J. C. Gay, Phys. Rev. Lett. **66**, 145 (1991).
[5] H. Friedrich and D. Wintgen, Phys. Rep. **183**, 37 (1989).
[6] P. Fassbinder and W. Schweizer, Phys. Rev. A **53**, 2135 (1996); M. Robnik, J. Phys. A **14**, 105 (1977); J. L. Greenstein and J. B. Oke, Astrophys. J. **252**, 285 (1982); G. Wunner, H. Ruder, and H. Herold, Phys. Lett. **79A**, 159 (1980); **247A**, 374 (1981).
[7] C. M. Dai and D. S. Chu, Physica B **172**, 445 (1991); A. K. Ramdas and S. Rodriguez, Rep. Prog. Phys. **44**, 1297 (1981); H. S. Brandi, Phys. Rev. A **11**, 1835 (1975); J. G. Mavroides, *Optical Properties of Solids*, edited by F. Abeles (North-Holland, Amsterdam, 1972); G. E. Stillman, D. M. Larsen, C. M. Wolfe, and R. C. Brandt, Solid State Commun. **9**, 2245 (1971); H. Hasegawa, *Physics of Solids in Intense Magnetic Fields* (Plenum, New York, 1969).
[8] J. C. Gay, Comments At. Mol. Phys. **25**, 185 (1991); J. Main and G. Wunner, J. Phys. B **27**, 2835 (1994); D. Delande, *Chaos and Quantum Physics*, 1989 Les Houches Lectures Session LII, edited by M. J. Giannoni, A. Voos, and J. Zinn-Justin (North-Holland, Amsterdam, 1991); H. Friedrich, *Theoretical Atomic Physics* (Springer-Verlag, Berlin, 1991), Sec. 5.3.4; H. Hasegawa, M. Robnik, and G. Wunner, Prog. Theor. Phys. Suppl. **98**, 198 (1989).
[9] S. Watanabe and H. Komine, Phys. Rev. Lett. **67**, 3227 (1991); H. Hasegawa, M. Robnik, and G. Wunner, Prog. Theor. Phys. Suppl. **98**, 198 (1989); J. Main, G. Wiebush, A. Holle, and K. H. Welge, Phys. Rev. Lett. **56**, 2594 (1986); J. C. Gay and D. Delande, *Atomic Excitation and Recombination in External Fields*, edited by M. H. Nayfeh and C. W. Clark (Gordon and Breach, New York, 1985); D. Kleppner, M. G. Littman, and L. Zimmerman, *Rydberg States of Atoms and Molecules*, edited by R. F. Stebbings and F. B. Dunning (Cambridge University Press, Cambridge, 1983).
[10] A. V. Sergeev (private communication).
[11] P. A. Braun and V. I. Savichev, J. Phys. B **26**, 3739 (1993); P. Cacciani, C. Delsart, E. Luckoenig, and J. Pinard, *ibid.* **25**, 1991 (1992); Q. Wang and C. Greene, Phys. Rev. A **44**, 1874 (1991); I. Sh. Averbukh and N. F. Perelman, Phys. Lett. A **139**, 449 (1989); G. R. Welch, M. M. Kash, C. Iu, L. Hsu, and D. Kleppner, Phys. Rev. Lett. **62**, 893 (1989); C. Iu, G. R. Welch, M. M. Kash, L. Hsu, and D. Kleppner, *ibid.* **63**, 1133 (1989); T. F. Gallagher, Rep. Prog. Phys. **51**, 143 (1988); J. Parker and C. R. Stroud, Phys. Rev. Lett. **56**, 716 (1986).
[12] L. Chen, M. Cheret, F. Roussel, and G. Spiess, J. Phys. B **26**, L437 (1993); D. Delande and J. C. Gay, Europhys. Lett. **5**, 303 (1988); J. Liang, M. Gross, P. Goy, and S. Haroche, Phys. Rev. A **33**, 4437 (1986); R. G. Hulet and D. Kleppner, Phys. Rev. Lett. **51**, 1430 (1983).
[13] H. Friedrich, *Theoretical Atomic Physics* (Springer-Verlag, Berlin, 1990).
[14] For a general discussion of the square-root branch point of physical systems see J. Goldberg and W. Schweizer, J. Phys. A **24**, 2785 (1991).
[15] The chaotic region is much harder to describe since avoided crossings are so close together that assigning a well-defined character to each energy level becomes impossible.
[16] It is technically incorrect to say that the character exchanges *at* the avoided crossing because the states close to the avoided crossing are actually made up of a superposition of the states that are used to label each energy level.
[17] L. D. Landau and E. M. Lifshitz, *Quantum Mechanics* (Pergamon, Oxford, 1977), Sec. 79.
[18] M. Dunn, D. K. Watson, J. R. Walkup, and T. C. Germann, J. Chem. Phys. **104**, 9870 (1996).
[19] E. A. Solov'ev, Zh. Eksp. Teor. Fiz. **81**, 1681 (1981) [Sov. Phys. JETP **54**, 893 (1981)]; S. Yu. Ovchinnikov and E. A. Solov'ev, Comments At. Mol. Phys. **22**, 69 (1988).
[20] *Dimensional Scaling in Chemical Physics*, edited by D. R. Herschbach, J. Avery, and O. Goscinski (Kluwer, Dordrecht, 1992).
[21] C. M. Bender, L. D. Mlodinow, and N. Papanicolaou, Phys. Rev. A **25**, 1305 (1982).
[22] Y. Y. Goldschmidt, Nucl. Phys. B **393**, 507 (1993); J. Rudnick and G. Gaspari, Science **237**, 384 (1987); R. A. Ferrell and D. J. Scalapino, Phys. Rev. A **9**, 846 (1974); A. J. Bray, J. Phys. A **7**, 2144 (1974); H. E. Stanley, Phys. Rev. **176**, 718 (1968); T. H. Berlin and M. Kac, *ibid.* **86**, 821 (1952).
[23] M. Dunn, T. C. Germann, D. Z. Goodson, C. A. Traynor, J. D. Morgan III, D. K. Watson, and D. R. Herschbach, J. Chem. Phys. **101**, 5987 (1994).
[24] V. S. Popov, V. D. Mur, A. V. Sergeev, and V. M. Weinberg, Phys. Lett. A **149**, 418 (1990); V. S. Popov, V. D. Mur, and A. V. Sergeev, *ibid.* **149**, 425 (1990); V. S. Popov, V. D. Mur, A. V. Shcheblykin, and V. M. Weinberg, *ibid.* **124**, 77 (1987).
[25] A. Chatterjee, Phys. Rep. **186**, 249 (1990).
[26] A. A. Belov, Yu. E. Lozovik, and V. A. Mandelshtam, Zh. Eksp. Teor. Fiz. **98**, 25 (1990) [Sov. Phys. JETP **71**, 12 (1990)].
[27] V. S. Popov and A. V. Sergeev, Phys. Lett. A **193**, 165 (1994).
[28] V. M. Vaĭnberg, V. S. Popov, and A. V. Sergeev, Zh. Eksp. Teor. Fiz. **98**, 847 (1990) [Sov. Phys. JETP **71**, 470 (1990)].
[29] *New Methods in Quantum Theory*, edited by C. A. Tsipis, V. S. Popov, D. R. Herschbach and J. Avery, NATO Conference Book Vol. 8 (Kluwer Academic, Dordrecht, 1996).
[30] T. C. Germann and S. Kais, J. Chem. Phys. **99**, 7739 (1993).
[31] L. J. Boya and R. Murray, Phys. Rev. A **50**, 4397 (1994); S. Kais and G. Beltrame, J. Phys. Chem. **97**, 2453 (1993); U. P. Sukhatme, B. M. Lauer, and T. D. Imbo, Phys. Rev. D **33**, 1166 (1986); R. S. Gangyopadhyay, R. Dutt, and Y. P. Varshni, *ibid.* **32**, 3312 (1985); D. Bollé and F. Gesztesy, Phys. Rev. A **30**, 1279 (1984); M. Sinha-Roy, R. S. Gangyopadhyay, and B. Dutta-Roy, J. Phys. A **17**, L687 (1984).
[32] S. M. Valone, Int. J. Quantum Chem. **49**, 591 (1994); S. Kais, D. R. Herschbach, N. C. Handy, C. W. Marray, and G. J. Laming, J. Phys. Chem. **99**, 417 (1993); G. F. Kventsel and J. Katriel, Phys. Rev. A **24**, 2299 (1981); N. H. March, *ibid.* **30**, 2936 (1984); **34**, 5106 (1986); J. Math. Phys. **26**, 554 (1985).
[33] A. A. Suvernev and D. Z. Goodson, Chem. Phys. Lett. **269**, 177 (1997); J. Chem. Phys. **107**, 4099 (1997).
[34] P. Serra and S. Kais, Phys. Rev. A **55**, 238 (1997); J. Phys. A **30**, 1483 (1997); Chem. Phys. Lett. **275**, 211 (1997); Phys. Rev. Lett. **77**, 466 (1996); J. P. Neirotti, P. Serra, and S. Kais, *ibid.* **79**, 3142 (1997); Chem. Phys. Lett. **260**, 302 (1996).
[35] T. C. Germann, D. R. Herschbach, and B. M. Boghosian, Comput. Phys. **8**, 712 (1994).
[36] J. R. Walkup *et al.* (unpublished).
[37] C. M. Bender and S. A. Orszag, *Advanced Mathematical Methods for Scientists and Engineers* (McGraw-Hill, New York, 1978), Chap. 8.
[38] L. D. Landau, Phys. Z. Sowjetunion **2**, 46 (1932); C. Zener, Proc. R. Soc. London, Ser. A **137**, 696 (1932).

[39] G. Arfken, *Mathematical Methods for Physicists* (Academic, San Diego, 1985), pp. 377 and 378.

[40] These branch points are not only the values of the parameter b where $E_+ = E_-$, but the energy functions $E_+(b)$ and $E_-(b)$ actually share this point. This may be shown by following a path that takes $b \rightarrow b$ and encloses one of the branch points. From Eq. (8) this path takes $E_\pm$ into $E_\mp$. Thus, by letting the distance of the path to the branch point tend to zero while ensuring that the path continues to enclose the branch point we see that the branch point is common to both E_+ and E_-. (For a more detailed discussion see, for example, Ref. [18].)

[41] W. D. Heiss and A. L. Sannino [J. Phys. A **23**, 1167 (1990)] have related the distribution of square-root branch points in matrix Hamiltonian problems to the appearance of quantum chaos in these systems.

[42] Although the two-level system we chose in our example was real valued, we note that complex-valued two-level systems also require that real-valued branch points exist at the same location as long as the Hamiltonian is Hermitian.

[43] T. C. Germann, D. R. Herschbach, M. Dunn, and D. K. Watson, Phys. Rev. Lett. **74**, 658 (1995).

[44] The algorithm of choice for calculating circular Rydberg states using dimensional perturbation theory is the matrix method, discussed in Ref. [23]. The matrix method algorithm was used in this research. Twentieth-order calculations using the matrix method take only about 3 min to compute on a SparcStation 20 workstation.

[45] E. Fermi, Z. Phys. **71**, 250 (1931); G. Herzberg, *Molecular Spectra and Molecular Structure V. II* (Van Nostrand Reinhold, New York, 1945), p. 215.

[46] Because we log scale both axes, the avoided crossing center is slightly displaced from where the narrowest approach of energy levels appears in the figures.

[47] In this research, converged energy levels are found by Padé summing Eq. (17).

[48] The avoided crossings that appear in the E-versus-$|m|$ spectrum are harder to find than those appearing in the E-versus-B spectrum. One reason for this is the leading $\tilde{E}_\infty$ in Eq. (17), which does not affect the dynamics of the problem (that is, which state is associated with each energy level), but because of its $|m|$ dependence tends to mask the appearance of the avoided crossing. Therefore, subtracting this term from the energy series does not affect where an avoided crossing appears, but makes the avoided crossing more visible. The subsequent energy series has a leading δ that is also a function of $|m|$ but, as in $\tilde{E}_\infty$, does not affect the dynamics of the problem. Therefore, we factor this term out of the series as well. The result is a rescaling of the series as $E(\text{rescaled}) = (\tilde{E} - \tilde{E}_\infty)/\delta$ whenever we calculate the energy with respect to changes in $|m|$. Also, for these cases we use total energies, not binding energies. Therefore, the vertical axes on such plots change accordingly.

[49] We used *quadratic* Padé summation to find the square-root branch points shown in the figures. See Ref. [18] and references therein.

[50] In this research the quantum numbers ν_1 and ν_2, denoting the characters of the states, are related to the low-field quantum numbers n and k (see Ref. [5] and references therein) by $|\nu_1, \nu_2\rangle = |n-k-|m|-1, k\rangle$, where k orders the states with respect to energy in each nth hydrogenic manifold in the low-B-field limit. (The higher the value of k, the lower the energy.) Wintgen and Friedrich [5,54] find that only states with k $(=\nu_2)$ quanta that differ by 2 can exhibit a broad avoided crossing. In this case the Fermi resonance condition associated with these avoided crossings implies that, for the $X:Y$ Fermi resonance, the ratio $2X:Y$ must be an integer. Since X must be larger than Y (ω_1 must be larger than ω_2) the only allowed Fermi resonance (other than the hydrogenic 1:1 Fermi resonance that occurs at $B=0$, not relevant to this discussion) that satisfies the $|\Delta k| = 2$ condition is the 2:1 Fermi resonance. Note from Table I that not even all 2:1 Fermi resonances satisfy this condition and thus are expected to be broad. Furthermore, only avoided crossings involving two vibrational states (large k) are broad, further reducing the number of broad avoided crossings of the 2:1 Fermi resonance.

[51] A. A. Kotze and W. D. Heiss [J. Phys. A **27**, 3059 (1994)] have related the distribution of square-root branch points of diamagnetic hydrogen in the complex-B plane to the appearance of quantum chaos in these systems.

[52] W. D. Heiss and W.-H. Steeb, J. Math. Phys. **32**, 3003 (1991).

[53] A. Bohm, *Quantum Mechanics: Foundations and Applications* (Springer-Verlag, New York, 1986), Sec. I.7 and Chap. XXI.

[54] D. Wintgen and H. Friedrich, J. Phys. B **19**, 1261 (1986).